VALIDATION OF AN EXPERIMENTALLY DERIVED UNCERTAINTY MODEL

K.B. Lim[*], *D.E. Cox*[†], *G.J. Balas*[‡] *and J-N. Juang*[§]

The results show that uncertainty models can be obtained directly from system identification data by using a minimum norm model validation approach. The error between the test data and an analytical nominal model is modeled as a combination of unstructured additive and structured input multiplicative uncertainty. Robust controllers which use the experimentally derived uncertainty model show significant stability and performance improvements over controllers designed with assumed ad hoc uncertainty levels. Use of the identified uncertainty model also allowed a strong correlation between design predictions and experimental results.

1 Introduction

In many engineering problems, a linear, time-invariant (LTI) and finite dimensional model, while satisfying known physical relationships, is still an approximation of a true plant. The need for robust control is often due to the corruption of the measurement data by the secondary effects of measurement noise, external disturbances, nonlinearities, and possible time variations. Although strictly speaking, robust control theory for nonlinear, time-varying systems should be applied under the above circumstances, it is currently not available. However, it has been shown that LTI-based robustness theory can handle a class of time varying and nonlinear uncertainties or effects via conic sector theory [1, 2, 3]. The hope is that a small set of LTI plants will be sufficient to describe these secondary effects.

A method has been proposed recently [4, 5] for calculating the smallest norm of the difference between the raw system identification data and the predicted value from a given nominal model. In particular, this minimum norm is calculated in closed form (to within a linear matrix equation) and holds for a general nominal/uncertainty structure in linear fractional transformation (LFT) form. Among all model validating plants about the nominal, this method defines the smallest subset of plants about the nominal which validates the given experimental data, hence the name, minimum norm model validation (MNMV).

This paper is an attempt to demonstrate and validate the MNMV approach for methodically constructing uncertainty models for a real application. As part of a validation, the uncertainty weights identified are used in redesigning the controller and comparing the experimental closed loop performance to controllers that assume ad hoc uncertainty levels. The feasibility of the method is investigated by applying it to the Large Angle Magnetic Suspension Test Fixture (LAMSTF) [6]. The LAMSTF is an experimental testbed located at NASA Langley Research Center for precision pointing control studies in support of large gap magnetic suspension technology. The LAMSTF system is open loop unstable, hence system uncertainty identification (UID) is performed closed loop.

An analytical model as derived in [7, 8, 9] is used as the nominal model in this study although an identified model can be obtained and used as a nominal model from the same UID data. In principle, it should not matter which nominal model to use so long as the set of plants can be described without stretching the uncertainty size. Hence, any nominal model provided it is not too far away from the true unknown system could be used. For example, an observer based system identification (ID) technique [10, 11, 12] may be used to construct a single best nominal model and the residual discrepancies between the raw system ID data and the nominal model are bounded by a structured uncertainty connection, assumed a priori [13, 14]. This would yield a P-Δ model for robust control design directly from empirical data.

The paper is organized as follows. Section 2 summarizes the method used in the determination of uncertainty models by MNMV approach. In Section 3, the LAM-

[*]Research Engineer, Guidance & Control Branch, Flight Dynamics & Control Division, MS 161, NASA Langley Research Center, Hampton, VA 23681, k.b.lim@larc.nasa.gov

[†]Research Engineer, Guidance & Control Branch, Flight Dynamics & Control Division, MS 161, NASA Langley Research Center, Hampton, VA 23681, d.e.cox@larc.nasa.gov

[‡]Associate Professor, Department of Aerospace Engineering & Mechanics, 107 Akerman Hall, 110 Union Street S.E., University of Minnesota, Minneapolis, MN 55455, balas@jette.aem.umn.edu, Member AIAA

[§]Principal Scientist, Structural Dynamics Branch, Structures Division, MS 230, NASA Langley Research Center, Hampton, VA 23681, j.juang@larc.nasa.gov, Fellow AIAA

STF system is described briefly and the experimental configuration and UID parameters are described. This is followed by results from UID experiments. Section 4 describes how a series of controllers are designed, tested and then compared in terms of stability robustness and disturbance rejection performance. Conclusions are given in Section 5.

2 Uncertainty ID Algorithm

The general form of the model structure is given in Figure 1. Using a bounded, but unknown structured

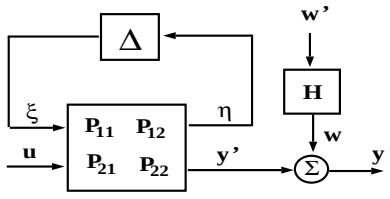

Figure 1: A priori model structure of plant in standard form

uncertainty model, a set of plants are defined that validates the available input-output data which contains the deviation or scatter about the nominal. The input-output relationship can be written as

$$y = F_u(P, \Delta)u + Hw' \tag{1}$$

where y, u, and w', denote the output, input and output noise. The upper LFT is defined by

$$F_u(P, \Delta) = P_{22} + P_{21}\Delta(I - P_{11}\Delta)^{-1}P_{12} \tag{2}$$

P denotes the augmented plant. The important point is that if the nominal P_{22} is known, the rest of the augmented plant can be constructed from a priori assumptions on the uncertainty structure. Note that H is the filter model for the noise and we let the uncertainty, Δ, to belong to the set of structured uncertainty $\mathcal{D}$, i.e., $\Delta \in \mathcal{D}$ [13].

Let the overall structured uncertainty be defined by the block diagonal matrices

$$\Delta = \text{diag}(\Delta^1, \ldots, \Delta^\tau); \quad \Delta^j \in C^{m_j \times n_j} \tag{3}$$

and the set of all block diagonal and stable, rational transfer function matrices be given by

$$\mathcal{D} = \left\{ \Delta(\cdot) \in RH_\infty : \ \Delta^j(s_o) \in C^{m_j \times n_j}, \forall s_o \in \bar{C}_+ \right\} \tag{4}$$

where τ and $\bar{C}_+$ denote the number of uncertainty blocks and the closed right-half plane, respectively [13]. We consider the class of problems where the uncertainty connections to the nominal and the plant inputs and outputs are given. In the next section, these deviations from a nominal model are used to develop unconservative frequency dependent structured uncertainty models.

To account for the discrepancies between the available measured outputs and feedback signals and their estimates from a nominal model, a priori knowledge of possible sources of uncertainties in the system are used. Figure 2 shows how a nominal model, P_{22} and an uncertainty connection structure can be used to define the LFT parameterized set of plants with output noise. The direct connection between the structured uncertainties, Δ, to the output and input mismatch, e^y and e^u is shown. These errors are defined by

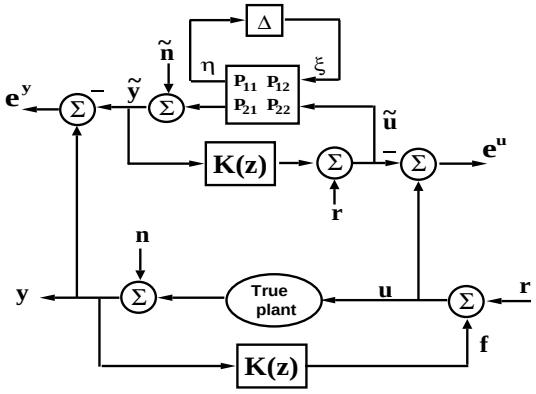

Figure 2: Configuration for system UID.

$$e := \left\{ \begin{array}{c} e^y \\ e^u \end{array} \right\} = \left\{ \begin{array}{c} y \\ u \end{array} \right\} - \left\{ \begin{array}{c} \tilde{y} \\ \tilde{u} \end{array} \right\} \tag{5}$$

It is important to note that the above errors are the residuals that remain after a single best model fit. This error time history is usually discarded in standard system ID applications. However, this residual error is precisely the data used in generating uncertainty models. It is clear that this error is composed of errors due to model mismatch and errors due to filtered noise. Note that the error expression in the estimated output for closed loop ID is the same as in the open loop [4].

The algorithm used to identify uncertainty bounds is given in [4] for open loop and in [5] for the closed loop case. In both cases, the norm of the smallest structured uncertainty that validates the available ID data at each frequency is found, i.e., a minimum norm model validation.

It is assumed that the controller dynamics, K, is known and the plant inputs, $u \in R^{n_u \times 1}$, and outputs, $y \in R^{n_y \times 1}$, are measured while the external command, $r \in R^{n_r \times 1}$ is selected. The fictitious signals in Figure 2 have dimensions $\eta \in C^{n_\eta}$ and $\xi \in C^{n_\xi}$ where

$$n_\eta = \sum_{j=1}^{\tau} n_j; \quad n_\xi = \sum_{j=1}^{\tau} m_j \tag{6}$$

The error in equation 5 is given by

$$e = e_o - R_{21}\Delta(I - R_{11}\Delta)^{-1}M_{12} \tag{7}$$

where

$$R_{11} = F_l(P,K) \tag{8}$$

$$R_{12} = P_{12}(I - KP_{22})^{-1}[I \quad K] \tag{9}$$

$$R_{21} = \begin{bmatrix} I \\ K \end{bmatrix}(I - P_{22}K)^{-1}P_{21} \tag{10}$$

$$R_{22} = \begin{bmatrix} (I - P_{22}K)^{-1}P_{22} & (I - P_{22}K)^{-1} \\ (I - KP_{22})^{-1} & (I - KP_{22})^{-1}K \end{bmatrix} \tag{11}$$

$$e_o = \begin{Bmatrix} y \\ u \end{Bmatrix} - R_{22}\begin{Bmatrix} r \\ \tilde{n} \end{Bmatrix} \tag{12}$$

$$M_{12} = R_{12}\begin{Bmatrix} r \\ \tilde{n} \end{Bmatrix} \tag{13}$$

Note that e_o is the residual from nominal fit when $\Delta = 0$. Define the above residuals at the discrete frequencies

$$\Omega = (z_1, \ldots, z_{n_\omega}); \quad z_j = e^{j\omega_i T} \tag{14}$$

by taking the discrete Fourier transform of both discrete time signals and systems.

Under conditions which ensure that a model validating solution exists, a solution to the MNMV problem is summarized as follows. A lower bound on the i-th component uncertainty at frequency z_j is given by

$$\bar{\sigma}(\Delta^i) = \|\Delta^i\|_2 \geq \frac{\|y^i\|_2}{\|x^i\|_2} \tag{15}$$

when $x^i \neq 0$, and

$$x := M_{12} + R_{11}(w + \phi); \qquad y := w + \phi \tag{16}$$

which are partitioned

$$x = \mathrm{col}\left(x^1, \ldots, x^\tau\right); \quad y = \mathrm{col}\left(y^1, \ldots, y^\tau\right) \tag{17}$$

in a conformal manner with respect to τ uncertainty blocks. The word "col" denotes a column vector formed from its arguments. Let $\mathcal{N}$ denote the null space of P_{21} and $\phi \in \mathcal{N}$. It has dimension $n_\xi - n_y$ and is spanned by the last $n_\xi - n_y$ columns of V. Let

$$w = P_{21}^{+}(I - P_{22}K)e_o^y \tag{18}$$

The singular value decomposition is given by

$$P_{21} = USV^* \tag{19}$$

where $U \in C^{n_y \times n_y}$ and $V \in C^{n_\xi \times n_\xi}$ are Hermitian matrices and $S \in R^{n_y \times n_\xi}$ is a full rank diagonal matrix. The pseudo-inverse is given by

$$P_{21}^{+} = VS^{+}U^* \tag{20}$$

A component uncertainty with this lower bound has been shown to exist. Thus the minimum norm bound δ^i for each uncertainty block can be computed from Eq.(15). For robust control design, the minimum bounds can be overbound by a stable, realizable low-order transfer functions for each uncertainty block.

3 Uncertainty ID of LAMSTF

A detailed description of the LAMSTF facility and the open-loop dynamic properties of the magnetic suspension system is given in [7]. Earlier studies on system ID and control for LAMSTF include [15, 8, 9, 16]. For LAMSTF, the model uncertainty is due to errors in the linearization about the equilibrium state, an inaccurate knowledge of the spatial distribution of the magnetic field, errors in the sensor system hardware, and errors at the plant input due to induced eddy currents.

3.1 Analytical Model

An analytical model is derived in [7, 8, 9] and reviewed only briefly here. Figure 3 show a schematic of the LAMSTF system. It basically consists of five electromagnets which actively suspend a small cylindrical permanent magnet. The cylinder is a rigid body and has five independent degrees of freedom, with motion in the roll axis being both unobserved and uncontrolled. Reference

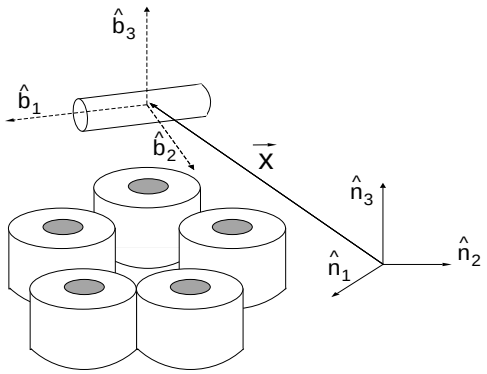

Figure 3: LAMSTF Configuration

[8] gives a detailed derivation of both the linear and nonlinear models. The following provides a synopsis for the linear model used in the control design.

By defining the state vector

$$\xi = (\omega_2, \omega_3,\ \beta_2, \beta_3,\ v_1, v_2, v_3,\ x_1, x_2, x_3)^T \tag{21}$$

the linearized perturbed motion about the equilibrium is given by

$$\dot{\delta\xi} = \hat{A}\delta\xi + \hat{B}\delta\rho \tag{22}$$

where the detailed expressions for $\hat{A}$ and $\hat{B}$ are given in [8]. Note that these analytical expressions depend on many physical constants including a series approximation of the magnetic field distribution. In fact, this field distribution and its frequency dependence due to eddy currents are believed to be the primary source of model errors. The variables ω_i, β_i, v_i, and x_i denotes ith angular velocity of cylinder with respect to body frame, ith Euler parameter relative to inertial frame, ith

Analytic Eigenvalues	Degree-of-Freedom
$0.00 \pm 0.95i$	z-axis
$0.00 \pm 7.97i$	x-axis,θ_y
± 9.77	y-axis
± 57.80	θ_z
± 58.78	θ_y, x-axis

Table 1: Eigenvalues of ten state analytic model

translational velocity and displacement of the centroid respectively. Six optical sensors detect in plane and out of plane motion, and provide an over-determined set of measurements for position in x, y, and z and rotation in pitch and yaw. The six optical sensors and five control coils yield a fully controllable and observable ten-state system whose eigenvalues are shown in Table 1.

The system's dynamics are dominated by the unstable pitch and yaw modes. These modes, called compass needle modes, result from the magnetic field being 180° out of phase with the cylinder's axial magnetization at the unstable equilibrium point. For a detailed discussion of the physical significance of all modes, the interested reader is referred to [7].

3.2 Uncertainty ID Experiment

The UID input test signal used consists of a frequency weighted, zero mean, white noise random signal for all five inputs, r (see Figure 2). This was generated by filtering a white noise signal with standard deviation of 1 (Ampere) through a fourth order low-pass Butterworth filter with break frequency of 60 Hertz. A second random signal with a bandwidth of 2 Hertz but with a standard deviation of 5 (Amperes) is added to the first wider bandwidth signal. This second signal is used to alleviate the lack of power at low frequencies which may result in a poor model at these low frequencies. The total time of the excitation signal is 40.96 seconds corresponding to 2^{13} discrete time points at 200 Hertz sampling rate.

Due to the closed loop coupling, the external UID signal introduced at the plant input is modified according to the unknown true input sensitivity transfer function matrix. Based on a nominal model, the top plot in Figure 4 show the input sensitivity matrix $T_{yr} = (I - F_u(P,\Delta)K)^{-1}$ while the bottom plot shows the closed loop transfer function across the plant $T_{yr} = (I - F_u(P,\Delta)K)^{-1}F_u(P,\Delta)$. Of course the true plant denoted by $F_u(P,\Delta)$ is not known so that the best model before the test is used. Figure 4 also show that the UID input is attenuated both at the input and output of the plant at low frequencies. This is due to the inherent disturbance rejection property of the controller used in the experiment. Note that the maximum singular value

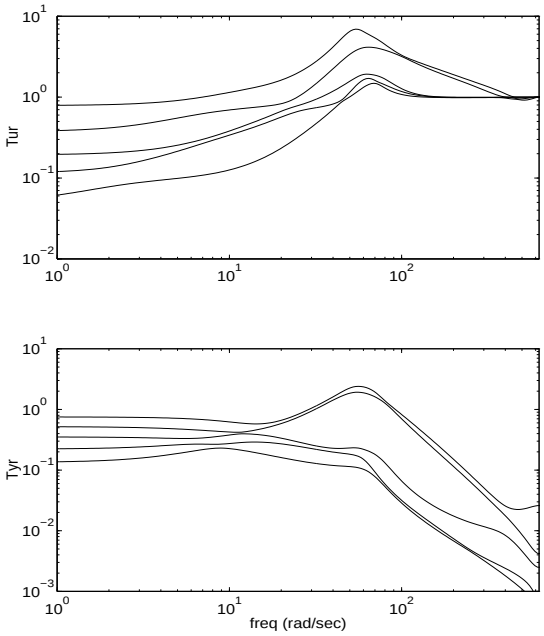

Figure 4: Singular values of input sensitivity (top) and closed-loop transfer function across plant (bottom).

at these low frequencies is an optimistic expectation of the actual response. The magnitudes of the input and outputs signals are largest at frequencies near 60 rad/sec. The output response to the UID signal is attenuated at higher frequencies. This means that an identified uncertainty will be limited in accuracy at both low and high frequencies

3.3 Uncertainty Model

It is known that in the LAMSTF system, there are several sources of uncertainties which include errors in the linearization about the equilibrium state, inaccurate knowledge of the spatial distribution of the magnetic field, errors in the sensor system hardware, and errors at the plant input due to induced eddy currents. For example, obtaining accurate analytical models of eddy currents using recently developed sophisticated computer code is challenging especially with multiple eddy current circuits with complex geometries [17].

In this study, we consider a combination of additive and structured input multiplicative uncertainty to describe the deviation of a nominal model. The reason for choosing this uncertainty structure is to give a sufficient degree of uncertainty freedom to permit a model validating solution. Of course in general, the selection of the uncertainty connections or structure is still an open issue.

Figure 5 shows the assumed connections for the uncertainties. The bounds on this structured uncertainty can then be experimentally determined by the minimum

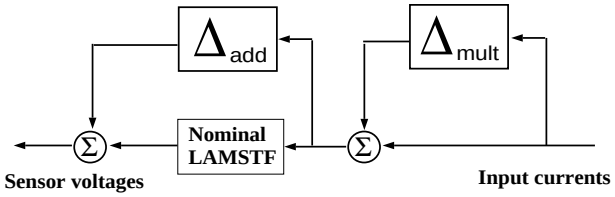

Figure 5: Assumed uncertainty structure.

norm model validation method. The $P-\Delta$ connections are given by

$$\left\{ \begin{array}{c} \xi_{add} \\ \xi_{mult} \end{array} \right\} = \left[\begin{array}{cc} \Delta_{add} & 0 \\ 0 & \Delta_{mult} \end{array} \right] \left\{ \begin{array}{c} \eta_{add} \\ \eta_{mult} \end{array} \right\} \qquad (23)$$

$$\left\{ \begin{array}{c} \eta_{add} \\ \eta_{mult} \\ y \end{array} \right\} = P \left\{ \begin{array}{c} \xi_{add} \\ \xi_{mult} \\ u \end{array} \right\} \qquad (24)$$

where the structured multiplicative uncertainty is

$$\Delta_{mult} = \mathrm{diag}(\delta_1, \ldots, \delta_5); \quad \delta_i \in C \qquad (25)$$

The augmented plant for the diagonal multiplicative uncertainty is

$$P = \left[\begin{array}{ccc} 0 & I & I \\ 0 & 0 & I \\ I & G & G \end{array} \right] \qquad (26)$$

The above variables have the following dimensions: $\xi_{add} \in C^{6\times 1}$, $\xi_{mult} \in C^{5\times 1}$, $\eta_{add} \in C^{5\times 1}$, $\eta_{mult} \in C^{5\times 1}$, $\Delta_{add} \in C^{6\times 5}$, $u \in R^{5\times 1}$, and $y \in R^{6\times 1}$.

The uncertainty bounds are calculated at discrete frequencies which are linearly spaced. A white noise signal having a spectral density of 10^{-6} is assumed for the presence of measurement noise. Since the number of uncertainty channels ($q = 11$) is greater than the number of outputs ($n_y = 6$), P_{21} is rectangular and its null space will be of minimum dimension 5. This means that the uncertainty bounds can be further reduced if this null space freedom is utilized. However, this freedom is not considered in this study.

Figure 6 shows the calculated minimum norm additive uncertainty at discrete frequency points over the whole range of Nyquist frequency. The curve fit was performed interactively using the $\mu-Tool$ [14] `drawmag` routine using a stable, rational, first-order transfer function (solid line). The maximum (dashed line) and minimum (dash-dot line) singular value response of the nominal plant are shown for comparison. It is seen that at frequencies below approximately 7 Hz, the uncertainty is less than the minimum singular value response indicating that the additive uncertainty levels are very small while at higher frequencies (above 7 Hz), the predicted additive uncertainty effect becomes more important. At frequencies beyond 60 Hz, predicted uncertainty is unreliable because the ID input signal is bandlimited.

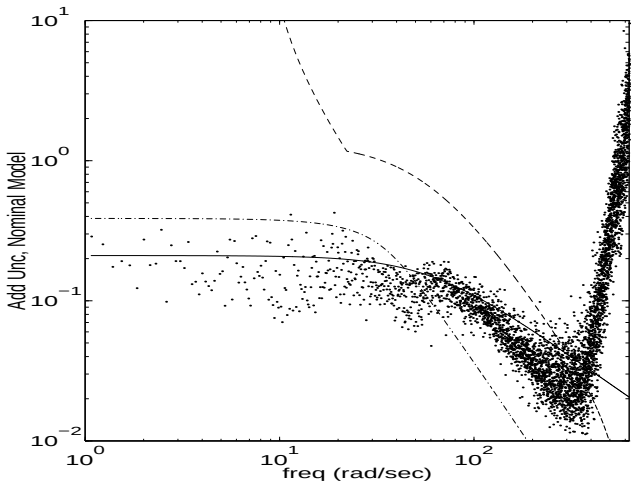

Figure 6: Additive Uncertainty: Predicted (dot), uncertainty fit (solid), maximum (dash) and minimum (dash-dot) singular value of nominal model

Figure 7 shows the calculated minimum norm multiplicative uncertainty (dot) and the corresponding second-order fit (solid line) for each input channel. The multiplicative uncertainty levels are generally larger at low frequencies and roll off with increasing frequencies.

Input channel number 1 shows largest uncertainty levels of up to about 90 % but at frequencies near crossover the uncertainty levels of all input multiplicative uncertainties are about 10 % or less. However, each channel appears to have different break frequencies for the roll off. For example, channel 1 having larger uncertainty levels at low frequencies than channel 2 rolls off at about 2 Hz as compared to about 10 Hz for channel 2. Note also that these experimentally based uncertainty predictions are very different when compared to assumed constant uncertainty levels. The consequence of this difference is evident from experimental results.

4 Performance Validation

The main objective of the control design is to stabilize the highly unstable open loop equilibrium configuration. Subject to closed loop stability, reasonable disturbance rejection performance across the plant is desired. Of course the above objectives are complicated by the presence of model error inaccuracies which are painfully evident during experiments. Hence, robust disturbance rejection is sought which requires a definition of the uncertainty set for which the performance is guaranteed. Uncertainty in the uncertainty model itself is a real dilemma which motivates this study which is a continuation of an earlier study [9]. Of course now we have the benefit of a new tool [4, 5] to more realistically capture model uncertainty.

Input	P_i	Z_i	k_i
1	-7.915 ± 12.26i	-19.80 ± 381.5i	1.127e-03
2	-22.57 ± 44.16i	-14.92 ± 430.2i	1.377e-03
3	-14.89 ± 17.74i	-15.78 ± 420.5i	1.294e-03
4	-13.92 ± 19.96i	-14.01 ± 418.3i	1.243e-03
5	-27.32 ± 49.56i	-30.91 ± 427.1i	1.115e-03

Table 2: Parameters for multiplicative uncertainty fit.

4.1 Controller Design

Figure 8 shows the interconnection used in the design of H_∞ and μ controllers [13]. The robust performance is defined by the principal gains such that

$$\bar{\sigma}\left[W_y(I - F_u(P,\Delta))^{-1}F_u(P,\Delta)\right] \leq 1; \forall\omega \in [0,\infty) \quad (27)$$

where the set of plants defined by the uncertainty,

$$\begin{aligned} \Delta &= \text{blk} - \text{diag}(\Delta_{add}, \Delta_{mult}) && (28)\\ \Delta_{add} &= \hat{\Delta}_{add} W_{add}; \qquad \bar{\sigma}(\hat{\Delta}_{add}) \leq 1 && (29)\\ \Delta_{mult} &= \hat{\Delta}_{mult} W_{mult}; \qquad \bar{\sigma}(\hat{\Delta}_{mult}) \leq 1. && (30) \end{aligned}$$

and the input multiplicative uncertainty has the diagonal form

$$\begin{aligned} \hat{\Delta}_{mult} &= \text{diag}(\hat{\delta}_1, \ldots, \hat{\delta}_5) && (31)\\ W_{mult} &= \text{diag}(w_{m1}, \ldots, w_{m5}) && (32) \end{aligned}$$

The additive uncertainties are fitted with the following first-order stable s-domain transfer function

$$W_{add} = 3.7708 \times 10^{-3} \frac{(s + 3380.7)}{(s + 60.615)} I_{5\times 5} \quad (33)$$

The multiplicative uncertainties are fitted with the following second-order stable transfer functions of the form

$$w_{m_i} = k_i \frac{(s + Z_i)(s + Z_i^*)}{(s + P_i)(s + P_i^*)}; \quad i = 1, \ldots, 5 \quad (34)$$

and the poles, zeros, and gains of the transfer functions are given in Table 2. The uncertainty weight for both additive and multiplicative case are subsequently discretized using the Tustin approximation of a continuous filter. The output performance weight, W_y, is chosen to be a constant diagonal matrix and equal for all six output channels.

To validate the experimentally derived uncertainty model, four sets of μ controllers are considered. Table 3 shows the four sets of controllers which were designed and tested. In all cases, the analytical model is used as the nominal model. The first two sets of controllers are based on unity output weights while the next two sets assume much smaller output weights of .1 and .01.

Contr	W_{unc}	W_y	μ_{des}	μ_{ID}	$\frac{\|y\|_2}{\|r\|_2}$	$\bar{\sigma}(T_{yr})$
C_{01}	.001	1	.17	5.44	U	
C_{02}	.1	1	1.89	2.89	0.29	2.69
C_{03}	.2	1	3.22	3.18	MU	
C_{04}	.3	1	4.57	3.48	MU	
C_{11}	IDed	1	1.56	1.56	0.19	1.40
C_{022}	.1	.1	1.41	5.63	U	
C_{023}	.1	.01	1.25	22.5	U	
C_{12}	IDed	.1	1.29	5.85	0.42	5.67
C_{13}	IDed	.01	1.23	28.5	0.84	26.4

Table 3: μ Control laws tested, U=Unstable, MU=Marginally Unstable.

The first set of control designs, C_{01},C_{02},C_{03}, and C_{04}, is based on assumed constant uncertainties at four different levels .001, .1, .2 and .3, respectively. The second control design, C_{11}, is based on an identified uncertainty model and uses the same unity output weight as the first set. A third set of controllers, C_{022} and C_{023}, are based on the assumed uncertainty level of .1 which was used to design controller C_{02} but with smaller output weights of .1 and .01 respectively. The fourth and last set of controllers, C_{12} and C_{13}, uses the scaled down output weights with the identified uncertainty weights.

4.2 Performance Comparison

In this subsection, we evaluate the validity of the identified uncertainty model by comparing predicted robust stability (RS) and robust performance (RP) to actual experimental results.

4.2.1 Stability Robustness

In the first set of control designs only controller C_{02}, which assumes uncertainty level of .1, was stable. Controller C_{01} was violently unstable while controllers C_{03} and C_{04} were marginally unstable, i.e., it built up oscillations slowly to eventually go out of range of the sensors. In contrast, a single control design, C_{11}, which is based on the identified uncertainty model, was stable and gave good performance without trial and error.

Based on the set of plants defined by the nominal and identified uncertainty model and the unity output weight, the predicted RS, nominal performance (NP), and RP were calculated for all nine controllers resulting to Figures 9 through 17. By comparing the predicted RS (solid line), the four controllers that were actually stable, C_{11},C_{12},C_{13},C_{02}, have the four best predicted RS levels with respect to the identified uncertainty.

The two marginally unstable controllers, C_{03},C_{04}, have slightly worse predicted RS levels than the least

stable controller, C_{02} among the four stabilizing controllers. This suggests that the true system uncertainly level, W^o_{unc}, lies in the narrow margin between C_{03} (or C_{04}) and C_{02}, i.e.,

$$\frac{W_{unc}}{\mu_{W_{unc}}([F_l(P,C_{03})]_{11})} \leq W^o_{unc} \leq \frac{W_{unc}}{\mu_{W_{unc}}([F_l(P,C_{02})]_{11})} \tag{35}$$

The most violently unstable controller, C_{01}, corresponds to the worst RS prediction as shown in solid line in Figure 9. This controller design practically ignores RS by assuming $W_{unc} = .001 \times I_{10\times 10}$. Note that since stability was attained in the four controllers in spite of a violation of RS condition (of less than unity) by a factor of up to 2 at lower frequencies, the identified uncertainty model is slightly conservative and the RS condition is only a sufficient condition for true stability. However, a larger violation of RS condition as in controllers C_{022}, C_{023}, and C_{01} (see Figures 14,15, and 9) results in an unstable closed loop system.

Motivated by the actual stability of controller C_{02}, controllers C_{022} and C_{023} were designed with reduced output weights which resulted in an improvement in the predicted RP in terms of μ_{des}. If the assumed uncertainty of .1 is an accurate model, then reducing the output weight should lead to improved RS. Instead, controllers C_{022} and C_{023} were unstable when implemented. This instability is however consistent with the predicted degradation of RS when evaluated with the identified uncertainty model as shown in Figures 14 and 15. In stark contrast, controllers C_{12} and C_{13} with reduced output weight were stable although the disturbance rejection performance is poor as intended. This low performance but robust stability for controllers C_{12} and C_{13} can be seen from Figures 16 and 17. Namely, the predicted poor RP is due to poor disturbance rejection at low frequency while good RS level is maintained. This means that the identified uncertainty model used in controllers C_{11}, C_{12}, and C_{13}, displays a property of an "accurate" uncertainty model, namely the RS condition should not depend on the choice of output weight.

4.2.2 Robust Performance

In Table 3, μ_{des} denotes the designed μ with respect to the particular uncertainty model (assumed or identified) and output weights. The value, μ_{ID} denotes the predicted μ based on the identified uncertainty model and the fixed unity output weight. Thus, the differences between μ_{des} and μ_{ID} values are solely due to the difference in both the uncertainty model assumed and the output weight. Therefore, μ_{des} equals μ_{ID} only for C_{11}.

Recall that a predicted RP is meaningful only with respect to the performance definition and the set of plants defined by the nominal and an uncertainty model. Clearly, if the set of plants assumed is in question, so is the reliability of the predicted robust performance. For instance, μ_{des} for controller C_{01} is the smallest at .17 (see Table 3) but when implemented, the closed loop system for this controller resulted in the most unstable system among the nine controllers tested. On the other hand, the best RP predicted by μ_{ID} is controller C_{11} at 1.56. When tested, this controller actually gave the best performance out of the nine controllers.

In order to experimentally validate the RP predictions, a system ID experiment was conducted on the disturbance to output path of the closed loop system. Identifying the system in this path allows the calculation of the worst case response, i.e., the maximum singular value over all frequencies. A wideband uncorrelated disturbance input was added to each of the control coils and measurements recorded from the system's sensors. This data was used with the OKID algorithm [10] to generate state-space models of the closed-loop system's disturbance path, denoted as T_{yr}. The maximum singular values were then calculated to obtain the identified worst case response subject to system ID limitations. This maximum singular values were directly compared to the predicted μ_{ID} bounds for robust performance. Figures 18, 19, 20, 21 show these comparisons for all four stabilizing controllers over all frequencies.

For the controller pair C_{02} and C_{11}, which have good RP, the experimental system had worst-case performance just below the predicted μ bound, as shown in Figure 18 and 19. This supports the earlier observations involving robust stability, namely, the identified uncertainty model was found to be slightly conservative so that the predicted μ is expected to be above the identified experimental worst case response. The consistency between the identified experimental worst case response and predicted worst-case performance (based on identified uncertainty model) makes a strong case for the "accuracy" of the uncertainty model. The second pair of controllers, C_{12} and C_{13} were dominated by RS constraints (see Figure 16, 17) and had poor predicted RP. However, even in these cases there is still a remarkable correlation between the predicted worst case performance, and the maximum singular values of the identified disturbance path, as shown in Figures 20 and 21.

The last two columns in Table 3 show the ratio of signal 2-norms between the wideband white noise disturbance and the outputs, $\frac{\|y\|_2}{\|r\|_2}$, and the maximum singular value of an identified model, T_{yr}. From Table 3 it can be seen that for all four stabilizing controllers, the following relation is satisfied:

$$\frac{\|y\|_2}{\|r\|_2} \ll \bar{\sigma}(T_{yr}) \approx \mu_{ID}; \tag{36}$$

The predicted and measured worst case response matches approximately while they clearly bound a particular ratio

of signal 2-norms.

5 Conclusions

This study demonstrated the use of a recently proposed algorithm for determining uncertainty models directly from system uncertainty identification test data. Overall, there was a strong correlation between actual and predicted robust stability and performance. Because the LAMSTF testbed is highly unstable in open loop and is sensitive to model errors, these results represent a significant experimental demonstration of the identified uncertainty model and subsequent robust controller performance. Hence we conclude that the results validate the identified uncertainty model.

Robust control design based on the identified uncertainty model produced significantly better performance in terms of stability and robust performance. Use of the identified uncertainty model also significantly improved predictability. This reduces the need to tweak around both performance and uncertainty weights in a robust control design and subsequent application for real systems to obtain satisfactory performance.

The robust stability and performance results indicate that the identified uncertainty was not overly conservative. However, the null freedom available for the sufficiently parameterized uncertainty freedoms, was not used to reduce the minimum norm uncertainty bound. Although the experimental results given in this study are based on a particular structure of uncertainty, namely, a combined additive and unstructured input multiplicative uncertainties, the system uncertainty identification methodology applies to the general LFT framework.

References

[1] Safonov, M.G., *Stability and robustness of multivariable feedback systems*, MIT Press, Cambridge Press, Massachusetts, 1980, chapter 2.

[2] Zames, G., "On the input-output stability of time-varying nonlinear feedback systems- Part I," *IEEE Transactions on Automatic Control*, vol. AC-11, no. 2, pp.228-238, April 1966.

[3] Waszak, M.R., "A methodology for computing uncertainty bounds of multivariable systems based on sector stability theory concepts," *NASA Technical Paper 3166*, April, 1992.

[4] Lim, K.B., Balas, G.J., and Anthony, T.C., "Minimum-norm model validating identification for robust control," AIAA Paper No. 96-3717.

[5] Lim, K.B., "Closed form solution for minimum norm model validating uncertainty," Submitted for review in *IEEE Transactions on Automatic Control* and 1997 ACC.

[6] Groom, N.J., "Description of the Large Gap Magnetic Suspension System (LGMSS) Ground-Based Experiment," *Technology 2000*, NASA CP-3109, Vol. 2, 1991, pp.365-377.

[7] Groom, N.J., and Britcher, C.P., "Open-Loop Characteristics of Magnetic Suspension Systems Using Electromagnets Mounted in a Planar Array," NASA-TP 3229, November 1992.

[8] Lim, K.B., and Cox, D.E., "Robust tracking Control of a Magnetically suspended Rigid Body," *2nd Int. Symp. on Magnetic Suspension Technology*, 1993.

[9] Lim, K.B., and Cox, D.E., "Experimental Robust Control Studies on an Unstable Magnetic Suspension System," *1994 American Control Conference.*

[10] Juang, J-N., Phan, M., Horta, L.G., Longman, R.W., "Identification of Observer/Kalman Filter Markov Parameters: Theory and Experiments," *Journal of Guidance, Control, and Dynamics*, vol.16, No.2, March-April 93, pp.320-329.

[11] Juang, J-N., Phan, M., "Identification of System, Observer, and Controller from Closed-Loop Experimental Data," *Journal of Guidance, Control, and Dynamics*, vol.17, No.1, Jan-Feb 94, pp.91-96.

[12] Juang, J-N., *Applied System Identification*, Prentice-hall, Inc., Englewood Cliffs, New Jersey, 1994, chapter 8.

[13] Stein, G., and Doyle, J.C., "Beyond singular values and loop shapes," *Journal of Guidance, Control, and Dynamics*, vol.14, No.1, Jan-Feb 91, pp.5-16.

[14] Balas, G.J., Doyle, J.C., Glover, K., Packard, A., and Smith, R., *μ-Analysis and Synthesis Toolbox, User's Guide*, The MathWorks, Inc., Natick, MA., 1995.

[15] Groom, N.J. and Schaffner, P.R., "An LQR Controller Design Approach for a Large Gap Magnetic Suspension System (LGMSS)," NASA TM-101606, 1990.

[16] Huang,J-K, and Cox, D.E., "Closed loop system ID" *CDC*, 1994.

[17] Britcher, C.P., and Groom, N.J., "Eddy current computations applied to magnetic suspensions and magnetic bearings," Proceedings of MAG '95: *Magnetic Bearings, Magnetic Drives and Dry Gas Seals Conference & Exhibition*, Aug 10-11, 1995, Alexandria, Virginia, pp.333-342.

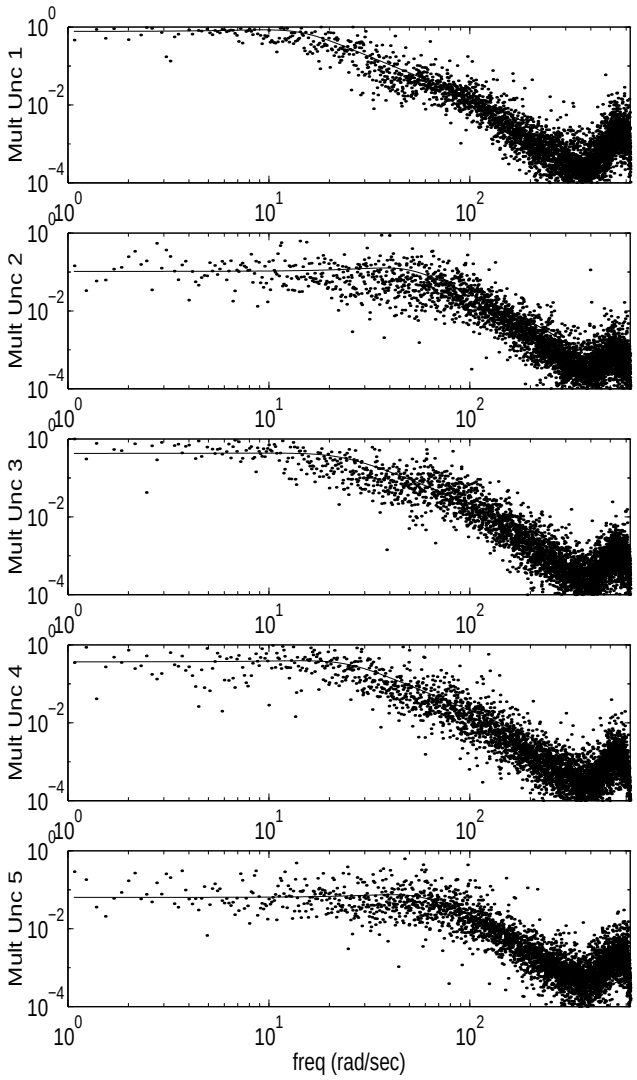

Figure 7: Input Multiplicative Uncertainty: Predicted (dot), uncertainty fit (solid).

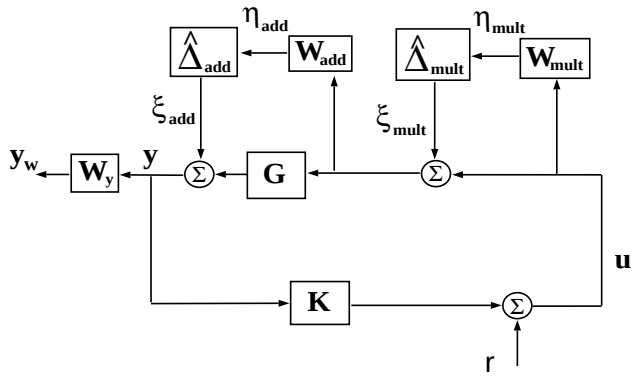

Figure 8: Interconnection for robust controller design.

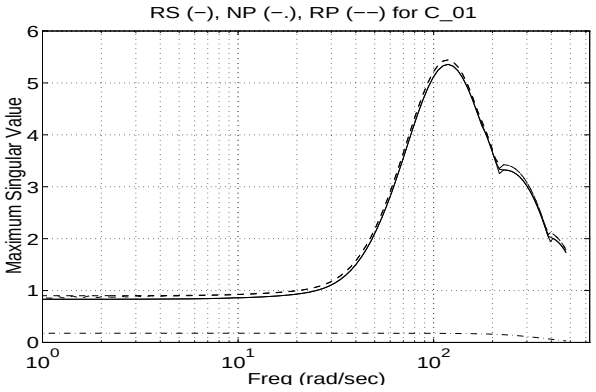

Figure 9: Predicted robust stability (solid), nominal performance (dash-dot), and robust performance (dash) for controller C_{01}.

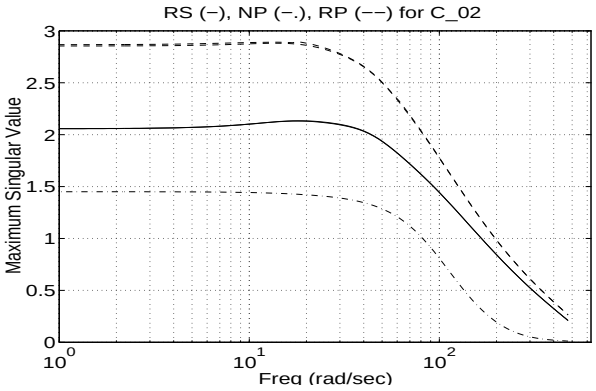

Figure 10: Predicted robust stability (solid), nominal performance (dash-dot), and robust performance (dash) for controller C_{02}.

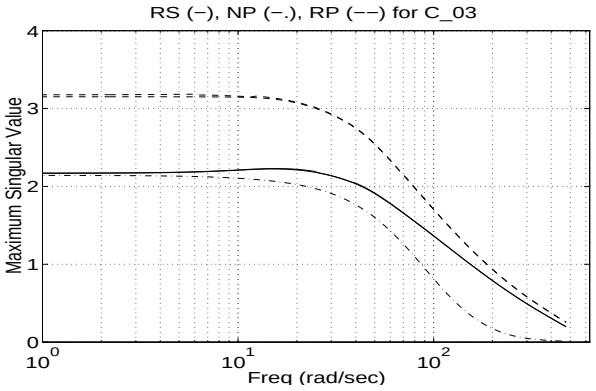

Figure 11: Predicted robust stability (solid), nominal performance (dash-dot), and robust performance (dash) for controller C_{03}.

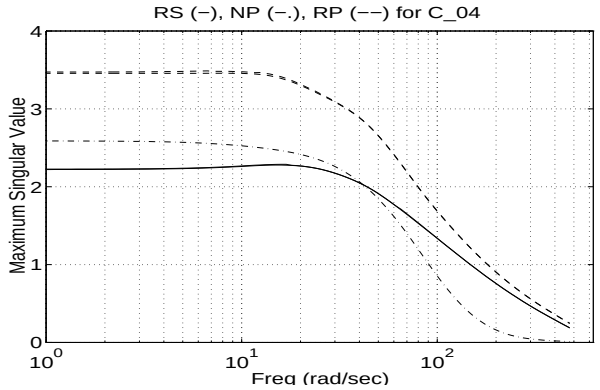

Figure 12: Predicted robust stability (solid), nominal performance (dash-dot), and robust performance (dash) for controller C_{04}.

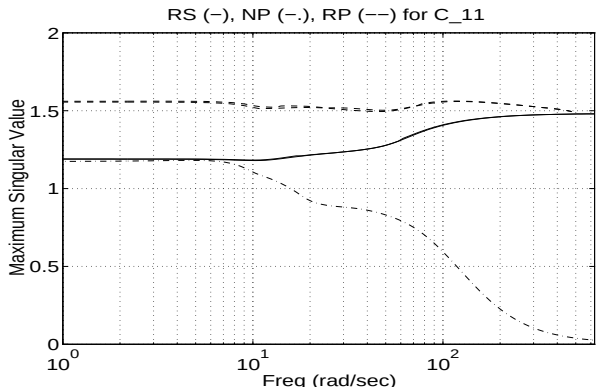

Figure 13: Predicted robust stability (solid), nominal performance (dash-dot), and robust performance (dash) for controller C_{11}.

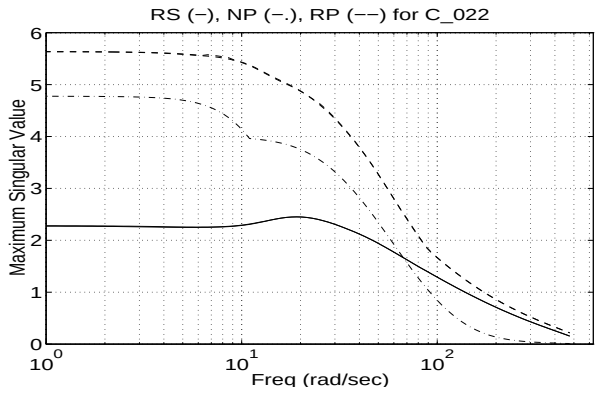

Figure 14: Predicted robust stability (solid), nominal performance (dash-dot), and robust performance (dash) for controller C_{022}.

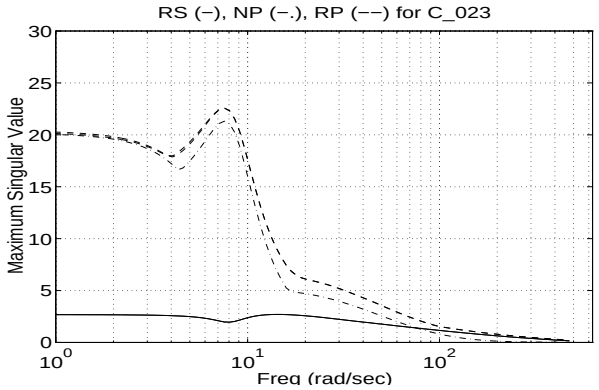

Figure 15: Predicted robust stability (solid), nominal performance (dash-dot), and robust performance (dash) for controller C_{023}.

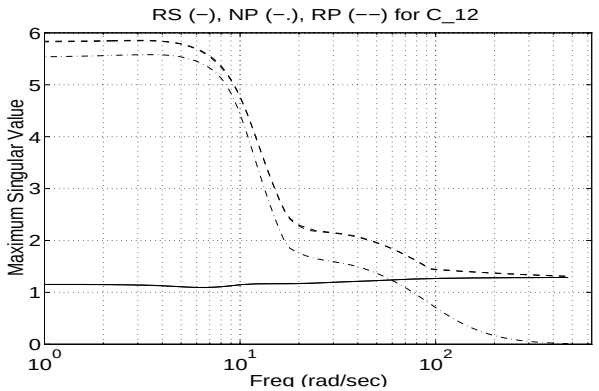

Figure 16: Predicted robust stability (solid), nominal performance (dash-dot), and robust performance (dash) for controller C_{12}.

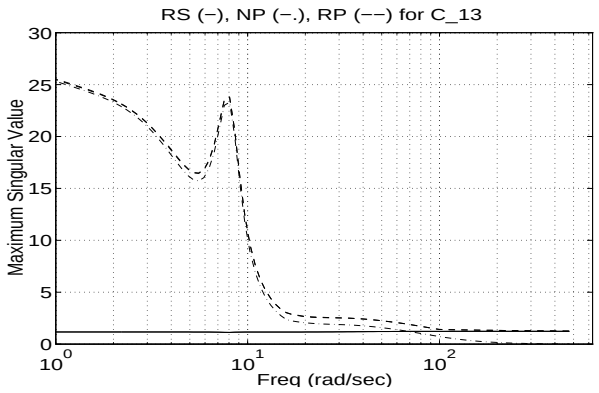

Figure 17: Predicted robust stability (solid), nominal performance (dash-dot), and robust performance (dash) for controller C_{13}.

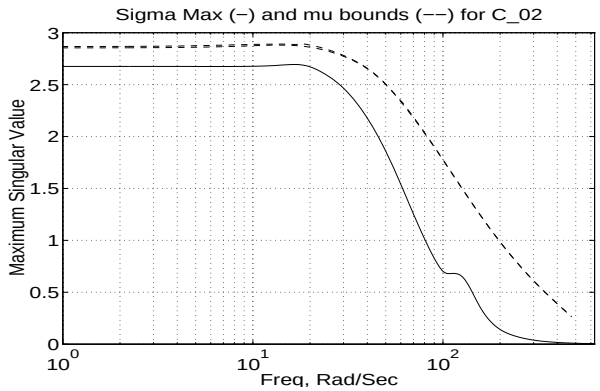

Figure 18: Identified worst case response (solid), predicted RP (dash) for controller C_{02}.

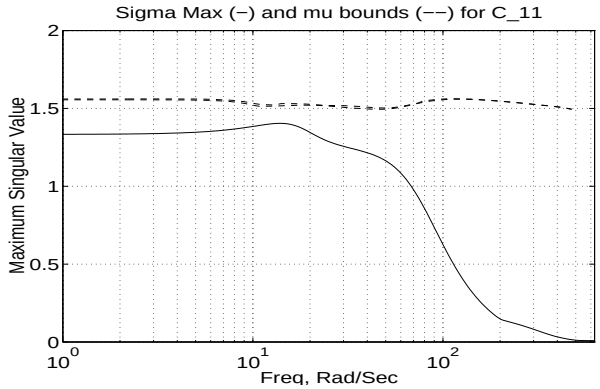

Figure 19: Identified worst case response (solid), predicted RP (dash) for controller C_{11}.

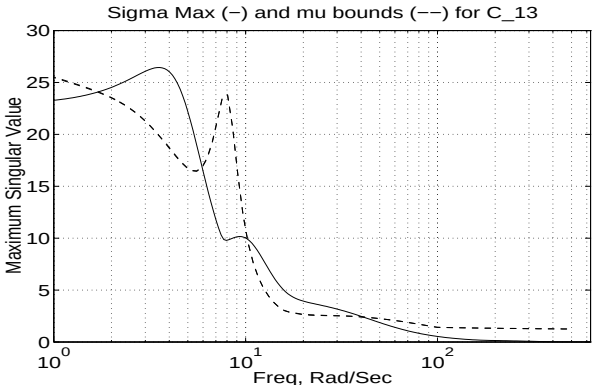

Figure 21: Identified worst case response (solid), predicted RP (dash) for controller C_{13}.

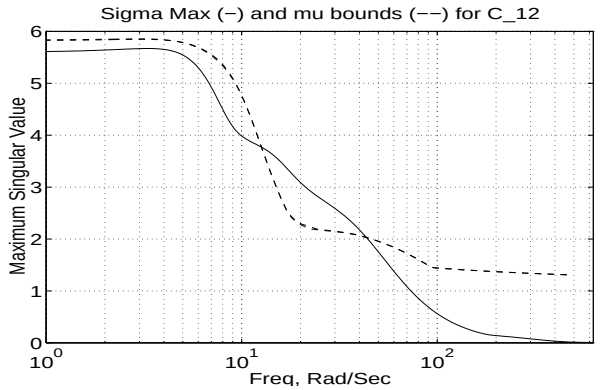

Figure 20: Identified worst case response (solid), predicted RP (dash) for controller C_{12}.